SCIENTIFIC JOURNAL
OF MARITIME RESEARCH
[POMORSTVO]

University of Rijeka
FACULTY OF MARITIME STUDIES

https://doi.org/10.31217/p.38.1.8

Isentropic and exergy analyses of marine steam turbine segments at several loads

Igor Poljak[1], Vedran Mrzljak[2*], Tomislav Senčić[2], Darko Pastorčić[1]

[1] University of Zadar, Department of Maritime Sciences, Mihovila Pavlinovića 1, 23000 Zadar, Croatia, e-mail: ipoljak1@unizd.hr; dpastorci@unizd.hr
[2] University of Rijeka, Faculty of Engineering, Vukovarska 58, 51000 Rijeka, Croatia, e-mail: vedran.mrzljak@riteh.uniri.hr; tomislav.sencic@riteh.uniri.hr
* Corresponding author

ARTICLE INFO

Original scientific paper
Received 8 May 2024
Accepted 3 June 2024

Key words:
Marine steam turbine
Turbine segments
Isentropic analysis
Exergy analysis
The ambient temperature variation
Various loads

ABSTRACT

This research presents isentropic and exergy analyses of marine steam turbine segments at three loads. Turbine segment is a part of any cylinder which is placed between the steam entrance to the cylinder and first steam extraction, between steam extractions and finally between last steam extraction and steam exit from the cylinder. Division of each cylinder to the segments allows insight into the various cylinder parts operation and an observation is the cylinder properly balanced. The analyzed marine steam turbine is composed of two cylinders – High Pressure Cylinder (HPC) and Low Pressure Cylinder (LPC), while each cylinder has two segments. The dominant part of real mechanical power produced in HPC is actually produced in the first HPC part (segment 1), while in LPC, the dominant part of real mechanical power is produced in the last LPC part (segment 4). Segments 1 and 3 have the highest improvement potential (inlet segments of both HPC and LPC) due to the highest isentropic losses and exergy destructions. HPC is much better balanced cylinder because along with isentropic, also exergy efficiencies between its segments (segment 1 and segment 2) at all loads differ lower than 7%, while the same cannot be stated for the LPC which exergy efficiencies between segments (segment 3 and segment 4) at all loads differ more than 20%. Very low isentropic and exergy efficiencies of the segment 3, at all observed loads, indicate that this turbine segment is highly problematic and at least some of the turbine stages mounted in this segment have difficulties in operation or potential malfunction. In addition, segment 3 is also the highest influenced by the ambient temperature change in comparison to other segments. The ambient temperature increase from 5 °C up to 45 °C can decrease segment exergy efficiency between 1.31% and 3.17%, if all the segments and all loads of the analyzed marine steam turbine are observed.

1 Introduction

Marine propulsion systems are nowadays dominantly based on the internal combustion engines which can be main propulsion engines (in the most of the cases slow speed two-stroke diesel engines) [1-6] or auxiliary engines (in the most of the cases medium or fast speed four-stroke diesel engines) [7-10]. In the literature can be found many numerical models for internal combustion engine simulation as well as various kinds of their operation improvement [11-16]. In addition, current legislation results in a notable reduction of harmful emissions from marine diesel engines, what requires various systems and techniques [17-19]. In the future, more stringent legislation related to marine internal combustion engines can be expected, so further improvements, additional systems and processes are surely required [20, 21].

Parallel to internal combustion engines, many marine propulsion alternatives are under the development at the moment [22, 23]. These marine propulsion alternatives are highly complex and requires proper investigation and analysis in various operating regimes before its final implementation [24-27]. Various complex numerical methods and processes for optimal propulsion alternative system selection can be found in the literature [28, 29].

Steam propulsion systems have still at the moment notable share in the propulsion of LNG (Liquefied Natural Gas) carriers worldwide [30-32]. However, internal combustion engines (dominantly dual fuel engines) are the most popular selection for a newly built LNG carriers, so it seems that in the future they will replace the most of steam propulsion systems [33-35].

In this paper are performed isentropic and exergy analyses of marine two cylinder steam propulsion turbine segments. Isentropic and exergy analyses are widely applied methods for the power systems and various components observation and optimization [36-40]. So far in the literature can be found various analyses of steam turbines and their cylinders [41, 42], but in the literature is not found any analysis which will observe different parts (segments) of any turbine cylinder. Therefore, the analyses performed in this paper will represent a guideline how different parts of any steam turbine cylinder can be observed. Also, the analyses related to the turbine segments allow more exact detection of problematic parts inside the steam turbine, which cannot be obtained by standard analyses.

2 Marine propulsion steam turbine description and operating regimes

The observed marine steam turbine is the main propulsor of one commercial LNG carrier [31]. The whole marine steam propulsion plant in which this turbine operates can be found in [43, 44]. Overall scheme of the steam turbine, turbine cylinders, segments and operating points required for the isentropic and exergy analyses, is presented in Fig. 1.

Marine steam turbine analyzed in this paper consist of two cylinders: High Pressure Cylinder (HPC) and Low Pressure Cylinder (LPC) [45]. Cumulative steam mass flow rate produced in two identical marine steam generators is delivered to the HPC which has one steam extraction. After steam expansion in the HPC, steam passes through the pipeline between HPC and LPC on which is mounted second steam extraction. A steam mass flow rate which is not extracted through first two extractions is delivered to the LPC through which expands again. As the HPC, LPC also has one steam extraction. The remaining steam mass flow rate expands

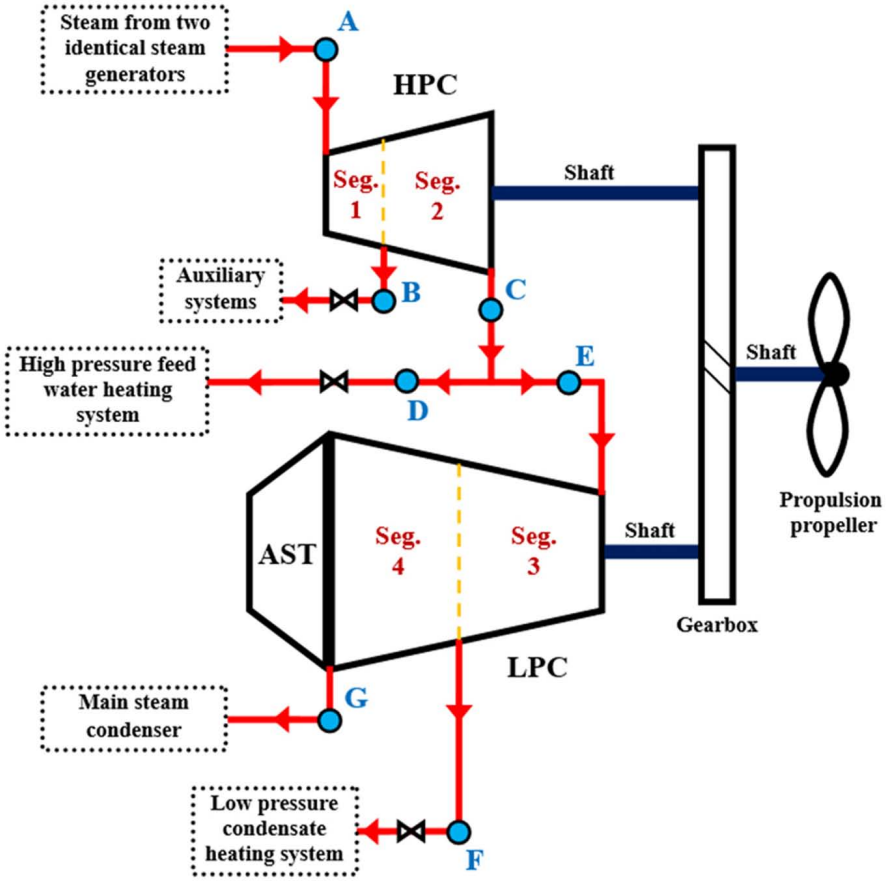

Figure 1 General scheme of the analyzed marine propulsion steam turbine and operating points necessary for the turbine segments analyses

Source: Authors

through the LPC outlet after which is delivered to the main steam condenser [46-48]. Each of three steam extractions on the observed turbine has regulating valves [49, 50] used for the exact extracted steam mass flow rate regulation. Both steam turbine cylinders are connected to the gearbox, which drives propulsion propeller [51, 52]. Inside the same cylinder along with the LPC is mounted steam turbine for the astern drive (AST, Fig. 1) which is usually composed of two Curtis stages [53], but it was not in operation at any load observed in this paper.

Observed turbine has four segments, as presented in Fig. 1. Turbine segment is a part of any cylinder which is placed between the steam entrance to the cylinder and first steam extraction, between steam extractions and finally between last steam extraction and steam exit from the cylinder. As can be seen from Fig. 1, both HPC and LPC of the observed turbine have two segments (between the steam entrance to each cylinder and steam extraction from each cylinder as well as between steam extraction from each cylinder and steam exit from each cylinder). Complex steam turbine cylinders with more than one steam extractions also have segments between each two steam extractions – an example of such cylinders can be found in [54]. Segments numeration is performed according to the steam flow through the turbine – the first segment is placed at the steam entrance in the HPC, while the last segment is placed at the steam outlet from LPC. Therefore, the turbine observed in this paper has four segments – segments 1 and 2 are related to the HPC, while segments 3 and 4 are related to the LPC. Standard isentropic and exergy analyses are dominantly performed for each turbine cylinder and whole turbine [55], while division of each turbine cylinder into segments allows that isentropic and exergy analyses can be also performed for at least two (or more) cylinder parts. The main goal of such division is to investigate the performance of various cylinder parts and consider its operation dynamics.

A maximal mechanical power which can be produced by this turbine (and delivered to the propulsion propeller) is equal to 29420 kW. The analyses performed in this paper are based on three turbine loads which correspond to around 80 – 85% of maximal load. During the LNG carrier exploitation, these were three the highest measured loads which correspond to the lowest specific fuel consumption in steam generators. Observed three loads are denoted throughout this paper as LOAD 1, LOAD 2 and LOAD 3, where the LOAD 1 is the lowest and LOAD 3 is the highest load. These three loads are not arbitrarily selected – only in these three loads all steam extractions are opened and through all extractions steam is delivered to steam consumers. At lower turbine loads, some steam extractions are closed (what depends on current plant operation dynamics). The closing of any steam extraction from HPC or LPC will result with a change of the cylinder segments, what was not an intention in the performed analyses (the intention was to maintain always the same, the maximal number of cylinder segments). For example, if the steam extraction from HPC is closed (steam mass flow rate through operating point B is equal to zero, Fig. 1) then in the HPC will remain only one segment (from the HPC inlet to the HPC outlet).

3 Isentropic and exergy analyses

3.1 Overall equations and balances

In this research, the isentropic and exergy analyses were utilized for the observation of marine steam turbine, its cylinders and cylinder segments. Both isentropic and exergy analyses were selected because each analysis considers different kind of losses, while in the exergy analysis can additionally be performed the investigation related to the ambient temperature change.

Isentropic analysis is completely independent of the ambient conditions [55]. Isentropic analysis of any turbine, turbine cylinder or cylinder segment is basically a comparison between real (polytropic) and ideal (isentropic) steam expansion processes [42, 56]. Real (polytropic) steam expansion process considers various losses which occur during steam expansion through turbine stages, and it is based on the steam operating parameters measured in the power plant during turbine exploitation [57]. In comparison to real (polytropic) steam expansion process, ideal (isentropic) expansion process is the process between the same pressures, with the same mass flow rates, but it assumes always the same steam specific entropy. Ideal (isentropic) expansion neglects all losses which occur during real steam expansion, and it represents theoretical, the best possible expansion process [42]. Therefore, in ideal (isentropic) steam expansion process, any turbine, turbine cylinder or cylinder segment will produce the highest possible (theoretical) mechanical power.

Real (polytropic) mechanical power produced in each turbine segment, turbine cylinder and whole turbine, respectively, is:

$$P_{\mathrm{PT,Seg,i}} = \dot{m}_{\mathrm{Seg,i}} \cdot (h_{\mathrm{in,Seg,i}} - h_{\mathrm{out,Seg,i}}), \tag{1}$$

$$P_{\mathrm{PT,cylinder,j}} = \sum_{\mathrm{i=1}}^{\mathrm{n}} P_{\mathrm{PT,Seg,i}}, \tag{2}$$

$$P_{\mathrm{PT,WT}} = \sum_{\mathrm{j=1}}^{\mathrm{k}} P_{\mathrm{PT,cylinder,j}}. \tag{3}$$

In the above equations, $\dot{m}$ is the fluid mass flow rate, P is mechanical power, h is fluid specific enthalpy, while the index PT represent real (polytropic) expansion, index i represent each individual segment, index j represent each individual cylinder, index *in* represents inlet (input), index *out* represents outlet (output), n is the number of cylinder segments and k is the number of turbine cylinders.

Ideal (isentropic) mechanical power of each turbine segment, turbine cylinder and whole turbine, respectively, is:

$$P_{\mathrm{IS,Seg,i}} = \dot{m}_{\mathrm{Seg,i}} \cdot (h_{\mathrm{in,Seg,i}} - h_{\mathrm{out,IS,Seg,i}}), \quad (4)$$

$$P_{\mathrm{IS,cylinder,j}} = \sum_{\mathrm{i=1}}^{\mathrm{n}} P_{\mathrm{IS,Seg,i}}, \quad (5)$$

$$P_{\mathrm{IS,WT}} = \sum_{\mathrm{j=1}}^{\mathrm{k}} P_{\mathrm{IS,cylinder,j}}, \quad (6)$$

where index IS represents ideal (isentropic) expansion process. The isentropic loss of each segment, cylinder and whole turbine is the difference between ideal and real mechanical power, while isentropic efficiency (of each segment, cylinder and whole turbine) is the ratio of real and ideal mechanical power.

In comparison to isentropic analysis which did not consider parameters of the ambient, exergy analysis considers ambient pressure and temperature [58, 59]. Therefore, exergy analysis requires definition of the base ambient state, but it also enables the ambient parameters change [60, 61].

The overall exergy balance equation for any control volume at steady state with negligible potential and kinetic energy changes is [62, 63]:

$$\dot{X} - P = \sum \dot{E}x_{\mathrm{out}} - \sum \dot{E}x_{\mathrm{in}} + \dot{E}x_{\mathrm{D}}. \quad (7)$$

In Eq. 7, $\dot{E}x_{\mathrm{D}}$ is exergy destruction, $\dot{X}$ is an exergy heat transfer at the temperature T, which can be defined by the equation [64]:

$$\dot{X} = \sum(1 - \frac{T_0}{T}) \cdot \dot{Q}, \quad (8)$$

where T is temperature and $\dot{Q}$ is energy heat transfer. Fluid exergy flow ,$\dot{E}x$ is [65]:

$$\dot{E}x = \dot{m} \cdot \varepsilon, \quad (9)$$

where fluid specific exergy ε is defined as [66, 67]:

$$\varepsilon = (h - h_0) - T_0 \cdot (s - s_0). \quad (10)$$

In Eq. 10, s is fluid specific entropy and index 0 is related to the ambient state. Always valid mass flow rate balance for any control volume is [68]:

$$\sum \dot{m}_{\mathrm{in}} = \sum \dot{m}_{\mathrm{out}}. \quad (11)$$

Overall exergy efficiency equation related to any control volume is [69]:

$$\eta_{\mathrm{ex}} = \frac{\text{cumulative exergy outlet}}{\text{cumulative exergy inlet}}. \quad (12)$$

3.2 Isentropic and exergy analyses of the observed marine steam turbine segments

Isentropic and exergy analyses of the marine steam turbine segments, cylinders and whole turbine are defined in accordance to the literature [68, 70-72]. At each of three observed turbine loads all equations remain the same (the change occurs in the fluid operating parameters only). Markings in the equations are defined according to operating points presented in Fig. 1 and Fig. 2.

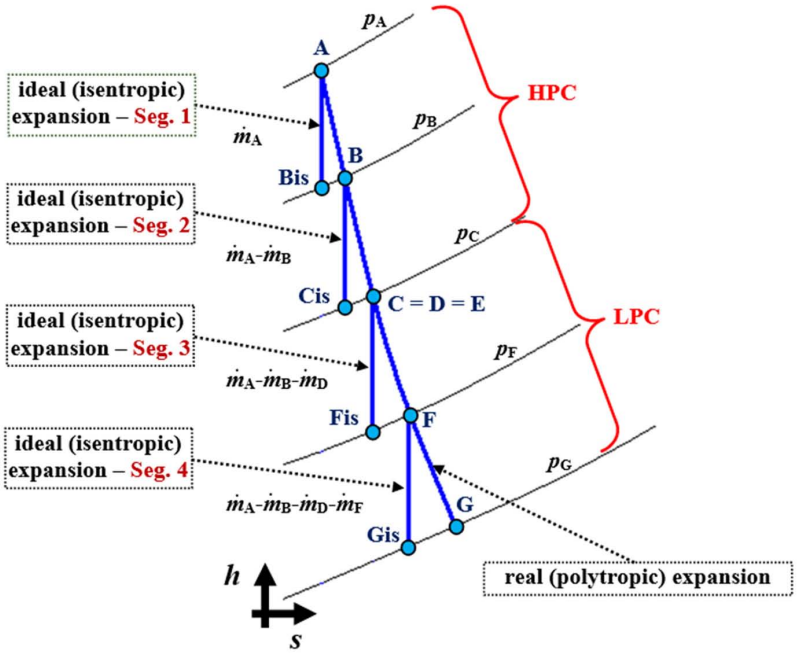

Figure 2 Ideal (isentropic) and real (polytropic) steam expansion processes in *h-s* diagram through each segment of the analyzed marine steam turbine

Source: Authors

In Fig. 2 is presented ideal (isentropic) and real (polytropic) steam expansion processes through each segment of the analyzed marine steam turbine in specific enthalpy-specific entropy (*h-s*) diagram. The operating points of the real (polytropic) steam expansion process in Fig. 2 remains identical as operating points presented in Fig. 1. It should be highlighted that operating point at the end of ideal (isentropic) steam expansion in each turbine segment has additional index – is, Fig. 2.

Equations for ideal (isentropic) and real (polytropic) mechanical power calculation of each turbine segment, cylinder and whole turbine are presented in Table 1, while equations for the isentropic loss and isentropic efficiency calculation of each turbine segment, cylinder and whole turbine are presented in Table 2.

Equations for the calculation of exergy inlet to each turbine segment and exergy outlet from each turbine segment are presented in Table 3.

Table 1 Equations for ideal (isentropic) and real (polytropic) mechanical power calculation of each turbine segment, cylinder and whole turbine

	Ideal (isentropic) mechanical power	Eq.	Real (polytropic) mechanical power	Eq.
Segment 1	$P_{\mathrm{IS,Seg,1}} = \dot{m}_{\mathrm{A}} \cdot (h_{\mathrm{A}} - h_{\mathrm{Bis}})$	(13)	$P_{\mathrm{PT,Seg,1}} = \dot{m}_{\mathrm{A}} \cdot (h_{\mathrm{A}} - h_{\mathrm{B}})$	(20)
Segment 2	$P_{\mathrm{IS,Seg,2}} = \dot{m}_{\mathrm{C}} \cdot (h_{\mathrm{B}} - h_{\mathrm{Cis}})$	(14)	$P_{\mathrm{PT,Seg,2}} = \dot{m}_{\mathrm{C}} \cdot (h_{\mathrm{B}} - h_{\mathrm{C}})$	(21)
Segment 3	$P_{\mathrm{IS,Seg,3}} = \dot{m}_{\mathrm{E}} \cdot (h_{\mathrm{E}} - h_{\mathrm{Fis}})$	(15)	$P_{\mathrm{PT,Seg,3}} = \dot{m}_{\mathrm{E}} \cdot (h_{\mathrm{E}} - h_{\mathrm{F}})$	(22)
Segment 4	$P_{\mathrm{IS,Seg,4}} = \dot{m}_{\mathrm{G}} \cdot (h_{\mathrm{F}} - h_{\mathrm{Gis}})$	(16)	$P_{\mathrm{PT,Seg,4}} = \dot{m}_{\mathrm{G}} \cdot (h_{\mathrm{F}} - h_{\mathrm{G}})$	(23)
HPC	$P_{\mathrm{IS,HPC}} = P_{\mathrm{IS,Seg,1}} + P_{\mathrm{IS,Seg,2}}$	(17)	$P_{\mathrm{PT,HPC}} = P_{\mathrm{PT,Seg,1}} + P_{\mathrm{PT,Seg,2}}$	(24)
LPC	$P_{\mathrm{IS,LPC}} = P_{\mathrm{IS,Seg,3}} + P_{\mathrm{IS,Seg,4}}$	(18)	$P_{\mathrm{PT,LPC}} = P_{\mathrm{PT,Seg,3}} + P_{\mathrm{PT,Seg,4}}$	(25)
WT	$P_{\mathrm{IS,WT}} = P_{\mathrm{IS,HPC}} + P_{\mathrm{IS,LPC}}$	(19)	$P_{\mathrm{PT,WT}} = P_{\mathrm{PT,HPC}} + P_{\mathrm{PT,LPC}}$	(26)

Source: Authors

Table 2 Equations for isentropic loss and isentropic efficiency calculation of each turbine segment, cylinder and whole turbine

	Isentropic loss	Eq.	Isentropic efficiency	Eq.
Segment 1	$L_{\mathrm{IS,Seg,1}} = P_{\mathrm{IS,Seg,1}} - P_{\mathrm{PT,Seg,1}}$	(27)	$\eta_{\mathrm{IS,Seg,1}} = \frac{P_{\mathrm{PT,Seg,1}}}{P_{\mathrm{IS,Seg,1}}}$	(34)
Segment 2	$L_{\mathrm{IS,Seg,2}} = P_{\mathrm{IS,Seg,2}} - P_{\mathrm{PT,Seg,2}}$	(28)	$\eta_{\mathrm{IS,Seg,2}} = \frac{P_{\mathrm{PT,Seg,2}}}{P_{\mathrm{IS,Seg,2}}}$	(35)
Segment 3	$L_{\mathrm{IS,Seg,3}} = P_{\mathrm{IS,Seg,3}} - P_{\mathrm{PT,Seg,3}}$	(29)	$\eta_{\mathrm{IS,Seg,3}} = \frac{P_{\mathrm{PT,Seg,3}}}{P_{\mathrm{IS,Seg,3}}}$	(36)
Segment 4	$L_{\mathrm{IS,Seg,4}} = P_{\mathrm{IS,Seg,4}} - P_{\mathrm{PT,Seg,4}}$	(30)	$\eta_{\mathrm{IS,Seg,4}} = \frac{P_{\mathrm{PT,Seg,4}}}{P_{\mathrm{IS,Seg,4}}}$	(37)
HPC	$L_{\mathrm{IS,HPC}} = L_{\mathrm{IS,Seg,1}} + L_{\mathrm{IS,Seg,2}}$	(31)	$\eta_{\mathrm{IS,HPC}} = \frac{P_{\mathrm{PT,HPC}}}{P_{\mathrm{IS,HPC}}}$	(38)
LPC	$L_{\mathrm{IS,LPC}} = L_{\mathrm{IS,Seg,3}} + L_{\mathrm{IS,Seg,4}}$	(32)	$\eta_{\mathrm{IS,LPC}} = \frac{P_{\mathrm{PT,LPC}}}{P_{\mathrm{IS,LPC}}}$	(39)
WT	$L_{\mathrm{IS,WT}} = L_{\mathrm{IS,HPC}} + L_{\mathrm{IS,LPC}}$	(33)	$\eta_{\mathrm{IS,WT}} = \frac{P_{\mathrm{PT,WT}}}{P_{\mathrm{IS,WT}}}$	(40)

Source: Authors

Table 3 Equations for exergy inlet and exergy outlet calculation of each turbine segment

	Exergy inlet	**Eq.**
Segment 1	$\dot{E}x_{\mathrm{in,Seg,1}} = \dot{m}_{\mathrm{A}} \cdot \varepsilon_{\mathrm{A}}$	(41)
Segment 2	$\dot{E}x_{\mathrm{in,Seg,2}} = (\dot{m}_{\mathrm{A}} - \dot{m}_{\mathrm{B}}) \cdot \varepsilon_{\mathrm{B}}$	(42)
Segment 3	$\dot{E}x_{\mathrm{in,Seg,3}} = \dot{m}_{\mathrm{E}} \cdot \varepsilon_{\mathrm{E}}$	(43)
Segment 4	$\dot{E}x_{\mathrm{in,Seg,2}} = (\dot{m}_{\mathrm{E}} - \dot{m}_{\mathrm{F}}) \cdot \varepsilon_{\mathrm{F}}$	(44)

	Exergy outlet	**Eq.**
Segment 1	$\dot{E}x_{\mathrm{out,Seg,1}} = \dot{m}_{\mathrm{B}} \cdot \varepsilon_{\mathrm{B}} + (\dot{m}_{\mathrm{A}} - \dot{m}_{\mathrm{B}}) \cdot \varepsilon_{\mathrm{B}} + P_{\mathrm{PT,Seg,1}}$	(45)
Segment 2	$\dot{E}x_{\mathrm{out,Seg,2}} = \dot{m}_{\mathrm{C}} \cdot \varepsilon_{\mathrm{C}} + P_{\mathrm{PT,Seg,2}}$	(46)
Segment 3	$\dot{E}x_{\mathrm{out,Seg,3}} = \dot{m}_{\mathrm{F}} \cdot \varepsilon_{\mathrm{F}} + (\dot{m}_{\mathrm{E}} - \dot{m}_{\mathrm{F}}) \cdot \varepsilon_{\mathrm{F}} + P_{\mathrm{PT,Seg,3}}$	(47)
Segment 4	$\dot{E}x_{\mathrm{out,Seg,4}} = \dot{m}_{\mathrm{G}} \cdot \varepsilon_{\mathrm{G}} + P_{\mathrm{PT,Seg,4}}$	(48)

Source: Authors

Exergy destruction and exergy efficiency of each turbine segment are calculated by using the following equations:

$$\dot{E}x_{\mathrm{D,Seg,i}} = \dot{E}x_{\mathrm{in,Seg,i}} - \dot{E}x_{\mathrm{out,Seg,i}}, \tag{49}$$

$$\eta_{\mathrm{ex,Seg,i}} = \frac{P_{\mathrm{PT,Seg,i}}}{\dot{E}x_{\mathrm{in,Seg,i}} - \dot{E}x_{\mathrm{out,Seg,i}} + P_{\mathrm{PT,Seg,i}}}, \tag{50}$$

where index i is related to each turbine segment (for the observed marine steam turbine with four segments, i = 1 – 4).

4 Marine steam turbine measurement results and measuring equipment

For the observed marine steam turbine isentropic and exergy analyses are required steam pressures, temperatures and mass flow rates in each operating point from Fig. 1 measured at each observed load during turbine exploitation. These operating points (and mentioned parameters) are also sufficient for both isentropic and exergy analyses of all turbine segments. From the measured temperatures and pressures in each operating point are calculated steam specific enthalpies and specific entropies by using NIST-REFPROP 9.0 software [73], while steam specific exergies are calculated by using Eq. 10.

All required steam data for the isentropic and exergy analyses, in each operating point from Fig. 1 at all three loads, are presented in the Appendix A at the end of this paper. Steam data at the lowest observed load (LOAD 1) are presented in Table A1, at LOAD 2 steam data are presented in Table A2, while at the highest observed load (LOAD 3) steam data are presented in Table A3.

Measurement results were obtained in ship exploitation, by using calibrated measuring equipment already mounted in ship engine room. Measuring equipment list is presented in the Table B1 placed in the Appendix B at the end of this paper.

The base ambient state for the exergy analysis can be selected provisionally, and there is no any rule for its selection [74]. In this paper, the base ambient state is defined with ambient pressure equal to 1 bar and ambient temperature equal to 25 °C.

5 Results and discussion

5.1 Results of the isentropic analysis

Real (polytropic) mechanical power produced in each turbine cylinder (HPC and LPC) as well as real (polytropic) mechanical power produced in the whole turbine (WT) at all three observed loads are presented in Fig. 3.

At each load, the sum of real mechanical power produced in segments 1 and 2 is real mechanical power produced in HPC, while the sum of real mechanical power produced in segments 3 and 4 is real mechanical power produced in LPC. Moreover, the sum of real mechanical power produced in both HPC and LPC at each observed load is real mechanical power produced in the whole turbine (WT).

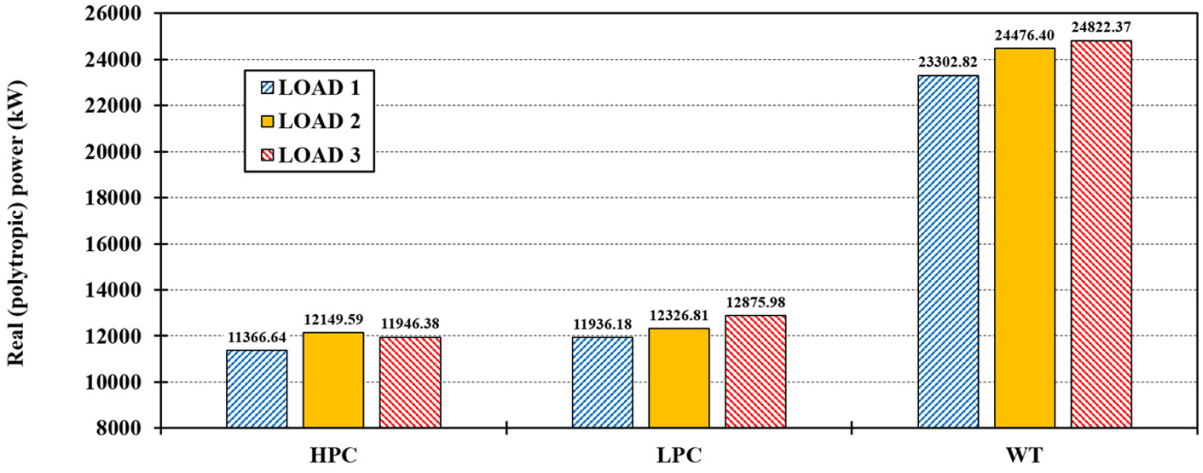

Figure 3 Real (polytropic) mechanical power produced in each turbine cylinder and in the whole turbine at three observed loads

Source: Authors

From Fig. 3 can be seen that at all loads observed in this paper real produced mechanical power in the whole turbine is almost equally divided on both HPC and LPC, what is not the case for this turbine at lower loads [75]. At all observed loads, real mechanical power produced in the LPC is only slightly higher than real mechanical power produced in the HPC.

As mentioned before, LOAD 1 is the lowest turbine load where real mechanical power produced in the whole turbine is equal to 23302.82 kW, while LOAD 3 is the highest load of all observed loads where real mechanical power produced in the whole turbine is 24822.37 kW.

Real (polytropic) mechanical power produced in each turbine segment at all observed loads is presented in Fig. 4.

From Fig. 4 can be concluded that HPC (segments 1 and 2) and LPC (segments 3 and 4) completely differ in real mechanical power production. The dominant part of real mechanical power produced in HPC is actually produced in the first HPC part (in segment 1), while in LPC, the dominant part of real mechanical power is produced in the second LPC part (segment 4). The first LPC part (segment 3) produces the lowest real mechanical power of all segments, while the last LPC part (segment 4) produces the highest real mechanical power of all

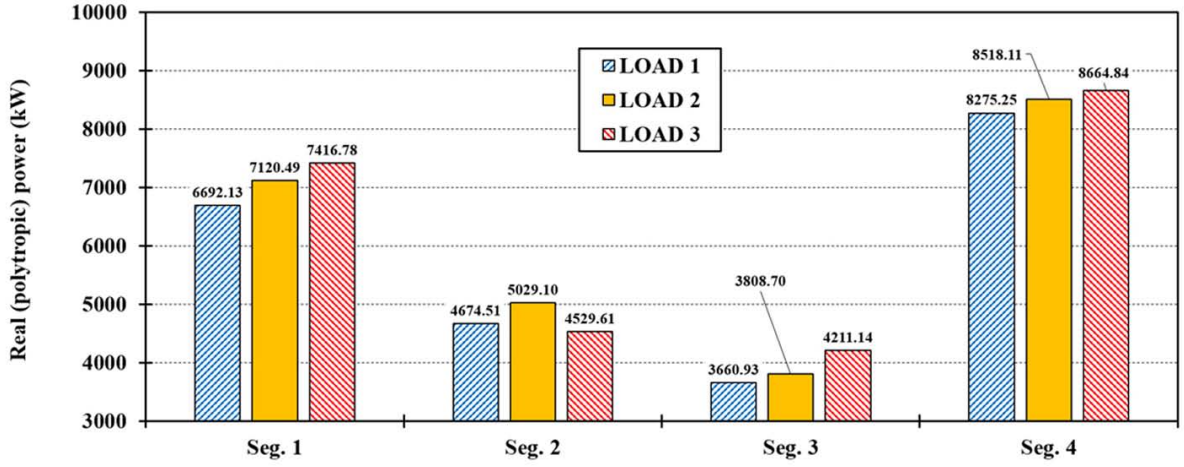

Figure 4 Real (polytropic) mechanical power produced in each turbine segment at three observed loads

Source: Authors

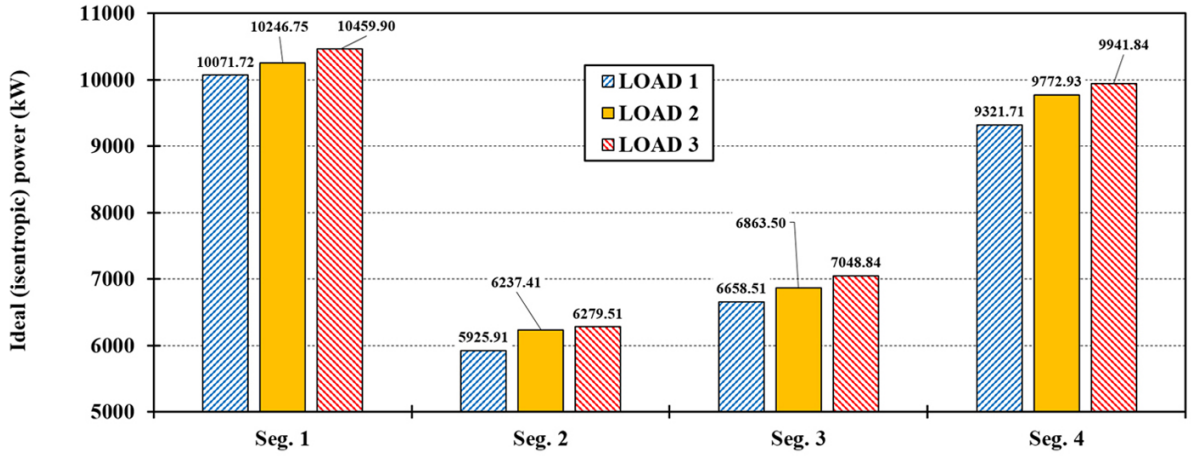

Figure 5 Ideal (isentropic) mechanical power which can theoretically be produced in each turbine segment at three observed loads

Source: Authors

segments, what is valid for all three observed loads. Therefore, from Fig. 3 where can be seen that real produced mechanical power in the whole turbine is almost equally divided to both turbine cylinders (at all observed loads), cannot be seen how the real mechanical power production is divided inside each cylinder (what is clearly presented in Fig. 4).

By observing all loads, in almost all segments real produced mechanical power increases from the lowest to the highest load (from LOAD 1 up to LOAD 3). The only exception can be seen in the segment 2, Fig. 4, where real produced mechanical power firstly increases during the load increase (from LOAD 1 to LOAD 2), while a further load increase (from LOAD 2 to LOAD 3) results with real produced mechanical power decrease.

For each turbine segment, at any observed load, ideal (isentropic) mechanical power is calculated according to *h-s* diagram from Fig. 2 and presented in Fig. 5.

Comparison of Fig. 4 and Fig. 5 shows that the trends related to the ideal mechanical power are not the same as the trends related to real power if observing all segments and loads. The same trend related to ideal and real mechanical power can be seen in a fact that the first HPC part (segment 1) produces significantly higher mechanical power in comparison to second HPC part (segment 2) as well as that the second LPC part (segment 4) produces notably higher mechanical power in comparison to the first LPC part (segment 3). However, segment 2 of the HPC is the segment in which can be produced the lowest ideal mechanical power of all segments (the lowest real mechanical power is produced in segment 3) at all loads, while the highest ideal mechanical power of all segments can be produced in segment 1 of the HPC (the highest real mechanical power is produced in segment 4 of the LPC) at all observed loads.

For all turbine segments, without any exception, is valid that the increase in load (from LOAD 1 up to LOAD 3) results with an increase in ideal mechanical power, Fig. 5.

Isentropic loss is the difference between ideal and real produced mechanical power. Isentropic loss actually shows how much more mechanical power can be produced in any segment, cylinder of whole turbine in comparison to the real produced mechanical power.

Isentropic losses of each segment from the observed marine steam turbine, at all three loads, are presented in Fig. 6. From Fig. 6 is clear that segments 1 and 3 have the highest improvement potential (inlet segments of both HPC and LPC) because in these segments occur the highest isentropic losses, much higher in comparison to the segments 2 and 4. From the isentropic aspect, any improvements which can potentially be performed in the observed marine steam turbine should be based firstly on the inlet parts of both cylinders. At all observed loads, segment 1 has the highest isentropic losses of all segments which are caused mainly by the steam of the highest pressure and temperature in the plant (produced in marine steam generators). At the HPC inlet, before steam expands through the turbine, are mounted main and regulating valves, so it can be concluded that improvements related to the regulating system can be very beneficial in reducing segment 1 (as well as the entire HPC) isentropic losses.

Isentropic loss and isentropic efficiency of turbine cylinders and whole turbine are reverse proportional. The same conclusion is valid for turbine segments, what is clear from the comparison of Fig. 6 and Fig. 7. Segments 1 and 3 which have the highest isentropic losses also have the lowest isentropic efficiencies. Segment 4 related to the last part of the LPC has the highest isen-

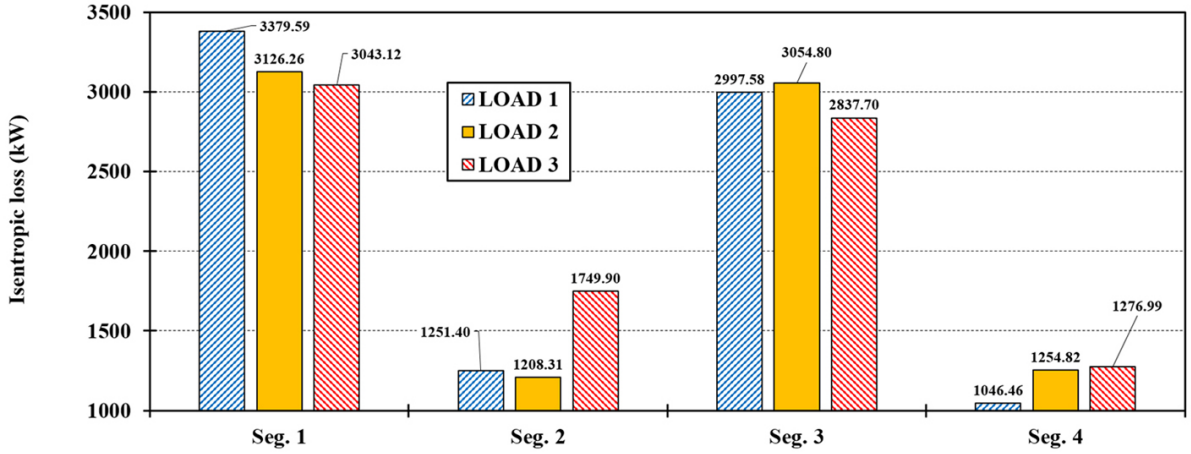

Figure 6 Isentropic loss of each turbine segment at three observed loads

Source: Authors

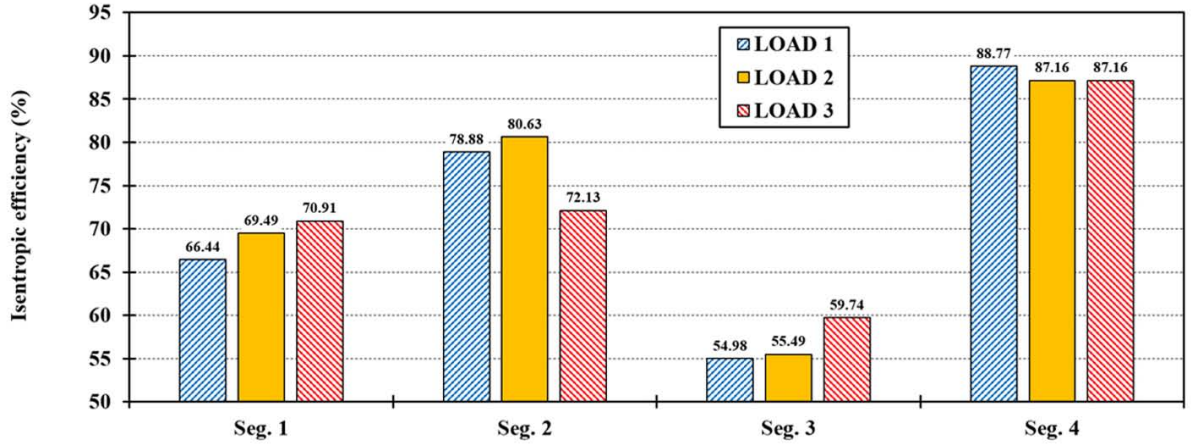

Figure 7 Isentropic efficiency of each turbine segment at three observed loads

Source: Authors

tropic efficiencies at all observed loads, which did not show significant variation during the load change. Also, the isentropic efficiencies show the fact that inlet segments of both turbine cylinders (HPC and LPC) have lower efficiencies in comparison to outlet segments.

By observing turbine cylinders at all loads, it can be seen that the differences between isentropic efficiency of segment 1 and segment 2 related to the HPC are around 10% or lower, while mentioned differences are extremely high by observing segment 3 and segment 4 of the LPC. In the LPC at all observed loads, isentropic efficiencies of inlet segment (segment 3) are around 30% lower than isentropic efficiencies of the outlet segment (segment 4). Isentropic efficiencies of the segment 3, Fig. 7, which are lower than 60% at all observed loads are highly problematic and indicate that at least some of the turbine stages mounted in this segment have difficulties in operation or potential malfunction.

It is very interesting that turbine stages mounted in the segment 4 (LPC outlet) show the best isentropic performance in comparison to all other segments. Mentioned turbine stages in segment 4 operates (at least partially) with wet steam which increases their inner losses, but that losses are obviously not highly influential to the segment isentropic efficiency.

5.2 Results of the exergy analysis

5.2.1 Exergy analysis results at the base ambient state

Exergy inlet to each turbine segment and exergy outlet from each turbine segment at all observed turbine loads for the base ambient state are presented in Fig. 8 and Fig. 9.

From Fig. 8 and Fig. 9 can be clearly seen that the trends in exergy inlet and outlet for the turbine segments at all observed loads are identical. Both exergy inlets and outlets are the highest at the turbine entrance (segment 1) and continuously decreases as the steam expands through the turbine. The last turbine segment (segment 4) operates with wet steam which has pressure notably lower than atmospheric pressure (in at least last few segment 4 stages) – such steam has low exergy flow and consequentially, segment 4 has the lowest exergy inlet and outlet.

An increase in turbine load from the lowest (LOAD 1) to the highest load (LOAD 3) results in continuous increase in exergy inlet and outlet of each turbine segment.

Observing turbine cylinders, it is easy to conclude that HPC has notably higher exergy inlets and outlets in comparison to LPC, due to much higher steam pressure and temperature which expands through the HPC.

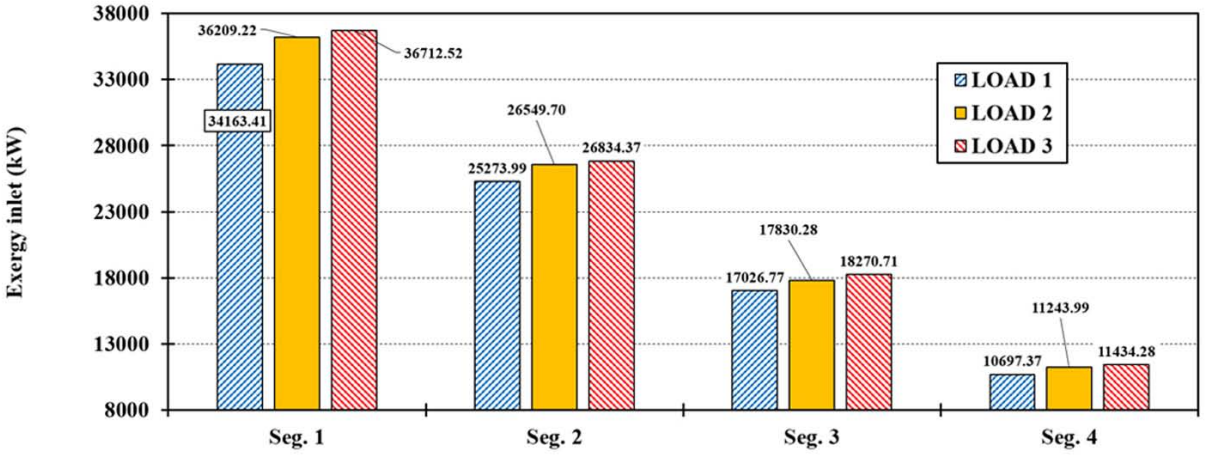

Figure 8 Exergy inlet of each turbine segment at three observed loads

Source: Authors

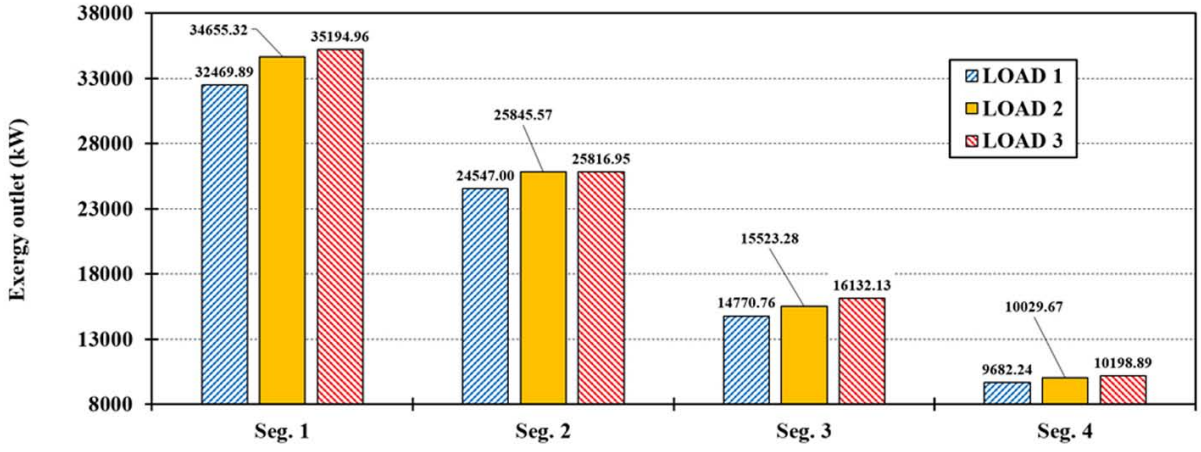

Figure 9 Exergy outlet of each turbine segment at three observed loads

Source: Authors

Exergy destructions of all turbine segments at each observed load are presented in Fig. 10. In comparison to isentropic losses (Fig. 6), exergy destructions of all segments show some similarities as well as some differences.

Both isentropic losses and exergy destructions are the highest at the first part of each turbine cylinder (segment 1 of the HPC and segment 3 of the LPC). Therefore, both isentropic losses and exergy destructions are not uniformly distributed in each part of any observed cylinder.

In comparison to isentropic loss which is the lowest in segment 4 at all observed loads, Fig. 6, exergy destruction is the lowest in segment 2 at all observed loads. Moreover, at all loads segment 3 has notably higher exergy destruction in comparison to all other segments, while the highest isentropic loss at all loads is observed in segment 1.

Differences between isentropic losses and exergy destructions show that isentropic and exergy analyses consider different kind of losses and that each analysis can detect different problematic turbine cylinders or segments.

Exergy efficiencies of each segment from the observed turbine at all loads are presented in Fig. 11. Both isentropic and exergy analyses (Fig. 7 and Fig. 11) show that the first LPC part (segment 3) has the worst performance in comparison to all other segments and consequentially the lowest isentropic and exergy efficiencies at all loads. Also the exergy analysis confirms conclusions from the isentropic analysis that at least some of the turbine stages mounted in segment 3 have difficulties in op-

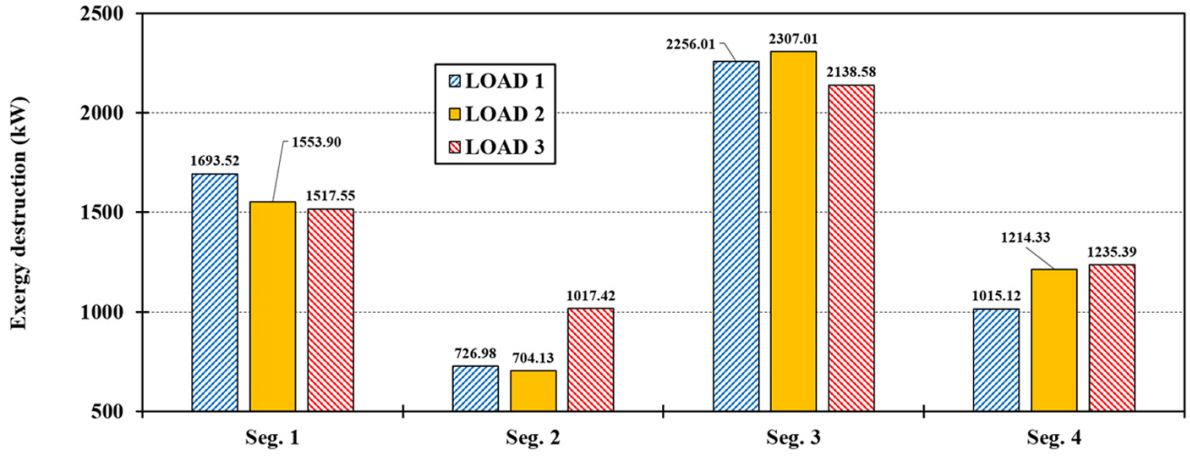

Figure 10 Exergy destruction of each turbine segment at three observed loads

Source: Authors

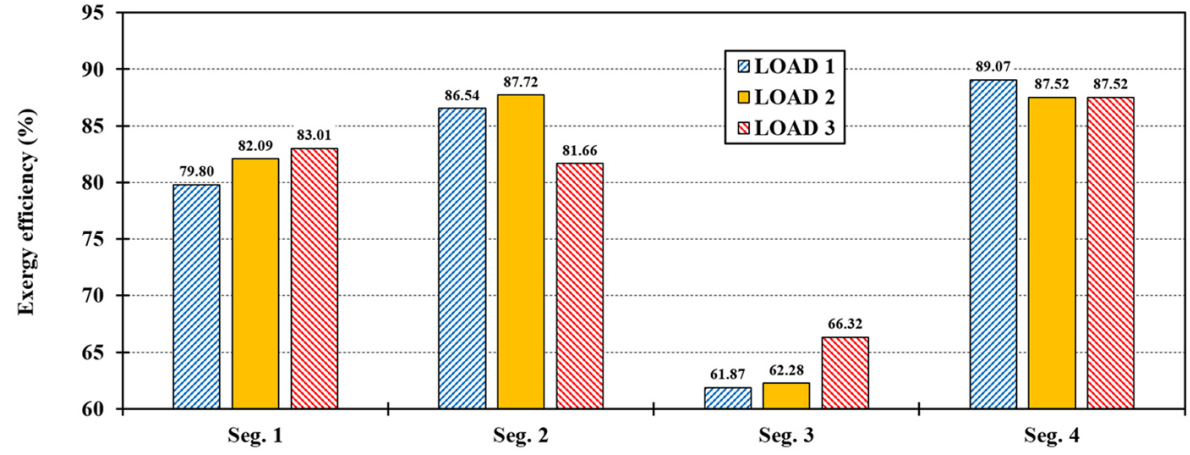

Figure 11 Exergy efficiency of each turbine segment at three observed loads

Source: Authors

eration or potential malfunction. Another confirmation of this fact can be seen in the second LPC part (segment 4) which has the highest isentropic and exergy efficiencies (Fig. 7 and Fig. 11) at all observed loads. Presented exergy efficiencies of segment 4 also highlights the fact that increased losses which occur in at least the last few segment 4 stages (due to wet steam) are not highly influential to the segment 4 efficiencies.

Comparison of observed turbine cylinders (HPC and LPC) also from the exergy aspect shows that HPC is much better balanced cylinder because exergy efficiencies between its segments (segment 1 and segment 2) at all loads differ lower than 7%. The same cannot be stated for the LPC which exergy efficiencies between segments (segment 3 and segment 4) at all loads differ more than 20%, Fig. 11.

5.2.2 Exergy analysis results during the ambient temperature variation

The last part of this research shows the investigation of the ambient temperature change influence on each turbine segment exergy destruction and exergy efficiency at all observed loads. In this research, the ambient temperature is varied from 5 °C up to 45 °C, while the ambient pressure remains the same as at the base ambient state (1 bar).

It should firstly be highlighted that an increase in the ambient temperature simultaneously increases exergy destruction and decrease exergy efficiency of each turbine segment at any observed load. The same is valid for the cylinders and the whole steam turbine [76, 77].

Increase in the exergy destruction of each turbine segment during the ambient temperature increase from 5 °C up to 45 °C at all observed loads is presented in Fig. 12. As proved before, segment 3 which shows the worst performance of all segments is also highly influenced by the ambient temperature change because its exergy destruction increases the most (in comparison to other segments). Inlet segments of both HPC and LPC are notably influenced by the ambient temperature change because its exergy destruction increase is notably higher in comparison to the outlet HPC and LPC segments. From the exergy destruction aspect, segment 2 is the lowest influenced by the ambient temperature change because during the increase in the ambient temperature exergy destruction of this segment has the lowest increase at all loads, Fig. 12.

Analysis of the turbine segments also shows that all parts of the same cylinder are not equally influenced by the ambient temperature change, what cannot be detected in the standard exergy analysis.

Decrease in exergy efficiency of each turbine segment during the ambient temperature increase from 5 °C up to 45 °C at all observed loads is presented in Fig. 13.

Segment 3 which has the lowest isentropic and exergy efficiencies at all loads (in comparison to the other segments) will also have the highest exergy efficiency decrease during the ambient temperature increase at all loads. This is another confirmation of the problematic stage's operation (or some of the stages) which are mounted in the segment 3. The lowest decrease in exergy efficiency of all segments can be seen in segment 4, Fig. 13, what is one more confirmation that LPC of the observed marine steam turbine is surely not properly balanced cylinder. The ambient temperature increase from 5 °C up to 45 °C can decrease exergy efficiency between 1.31% and 3.17%, if all the segments and all loads of the analyzed marine steam turbine are observed.

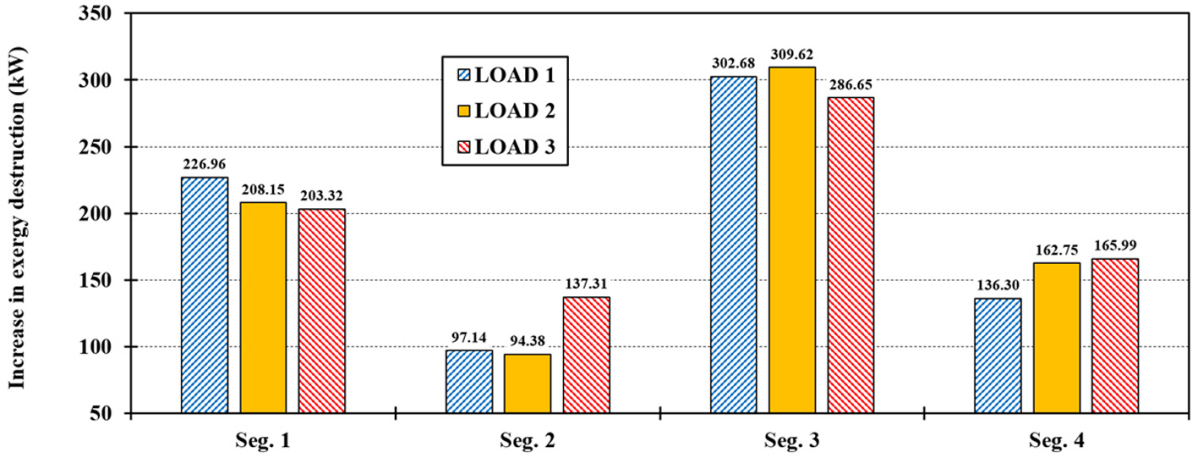

Figure 12 Increase in exergy destruction of each turbine segment at three observed loads during the ambient temperature increase from 5 °C up to 45 °C

Source: Authors

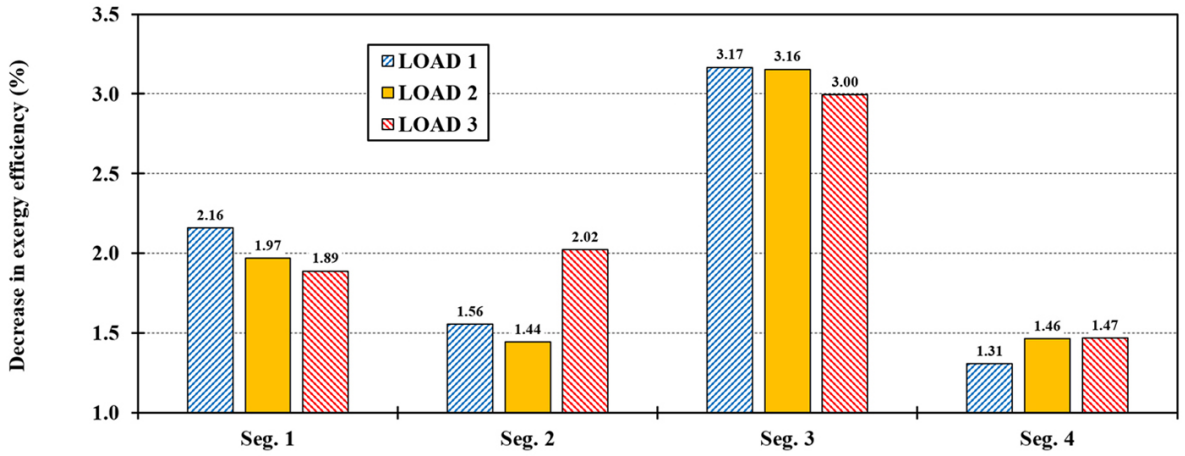

Figure 13 Decrease in exergy efficiency of each turbine segment at three observed loads during the ambient temperature increase from 5 °C up to 45 °C

Source: Authors

6 Conclusions

This paper presents isentropic and exergy analyses of marine steam turbine segments at three different loads. Turbine segment is a part of any cylinder which is placed between the steam entrance to the cylinder and first steam extraction, between steam extractions and finally between last steam extraction and steam exit from the cylinder. Obtained isentropic losses, exergy destructions as well as isentropic and exergy efficiencies can be a very helpful tool in detection of problematic cylinder parts (segments). Moreover, division of each cylinder to the segments allows insight into the various cylinder parts operation and an observation is the cylinder properly balanced or not. In addition, it is presented an analysis related to the ambient temperature change influence on each turbine segment exergy destructions and efficiencies. The most important conclusions obtained in the performed analysis are:

- At all turbine loads observed in this paper real produced mechanical power in the whole turbine is almost equally divided on both HPC and LPC, what is not the case for this turbine at lower loads.
- The dominant part of real mechanical power produced in HPC is actually produced in the first HPC part (segment 1), while in LPC, the dominant part of real mechanical power is produced in the second LPC part (segment 4). Real mechanical power produced in each turbine cylinder is not proportionally distributed to all cylinder segments.
- Segments 1 and 3 have the highest improvement potential (inlet segments of both HPC and LPC) due to the highest isentropic losses and exergy destructions. Therefore, both isentropic losses and exergy destructions are not uniformly distributed in each part of any observed cylinder.
- The differences between isentropic efficiency of segment 1 and segment 2 related to the HPC are around 10% or lower, while mentioned differences of segment 3 and segment 4 related to the LPC equals around 30% (observing all loads).
- HPC is much better balanced cylinder because along with isentropic, also exergy efficiencies between its segments (segment 1 and segment 2) at all loads differ lower than 7%. The same cannot be stated for the LPC which exergy efficiencies between segments (segment 3 and segment 4) at all loads differ more than 20%.
- Very low isentropic and exergy efficiencies of the segment 3, at all observed loads, indicate that this turbine segment is highly problematic and at least some of the turbine stages mounted in this segment have difficulties in operation or potential malfunction.
- It is very interesting that turbine stages mounted in the segment 4 (LPC outlet) show the best isentropic and exergy performance in comparison to all other segments. Mentioned turbine stages in segment 4 operates (at least partially) with wet steam which increases their inner losses, but that losses are not highly influential to the segment isentropic and exergy efficiencies.
- Turbine segment 3 which shows the worst performance of all segments is also highly influenced by the ambient temperature change because during the ambient temperature increase, exergy destruction of the segment 3 will increase and exergy efficiency will decrease much higher in comparison to other segments at all observed loads.
- The ambient temperature increase from 5 °C up to 45 °C can decrease segment exergy efficiency between 1.31% and 3.17%, if all the segments and all loads of the analyzed marine steam turbine are observed.

Appendix A – steam operating parameters at all observed loads

Table A1 Steam operating parameters at LOAD 1

Operating Point*	Temperature (°C)	Pressure (bar)	Mass flow rate (kg/s)	Specific enthalpy (kJ/kg)	Specific entropy (kJ/kg·K)	Quality	Specific exergy (kJ/kg)**	Isentropic specific enthalpy (kJ/kg)
A	501	59.11	24.832	3426.5	6.8936	Superheated	1375.80	-
B	354	14.86	0.485	3157.0	7.1222	Superheated	1038.10	3020.9
C	253	5.68	24.346	2965.0	7.2221	Superheated	816.24	2913.6
D	253	5.68	3.486	2965.0	7.2221	Superheated	816.24	-
E	253	5.68	20.860	2965.0	7.2221	Superheated	816.24	-
F	157	1.14	0.774	2789.5	7.5851	Superheated	532.59	2645.8
G	34.58	0.055	20.086	2377.5	7.7547	0.923***	70.05	2325.4

* According to Fig. 1 and Fig. 2

** At the base ambient state (ambient pressure = 1 bar, ambient temperature = 25 °C)

*** Quality of 0.923 denotes 92.3% of steam and 7.7% of water droplets

Table A2 Steam operating parameters at LOAD 2

Operating Point*	Temperature (°C)	Pressure (bar)	Mass flow rate (kg/s)	Specific enthalpy (kJ/kg)	Specific entropy (kJ/kg·K)	Quality	Specific exergy (kJ/kg)**	Isentropic specific enthalpy (kJ/kg)
A	500	57.95	26.382	3425.5	6.901	Superheated	1372.50	-
B	354	15.58	0.944	3155.6	7.099	Superheated	1043.70	3037.1
C	250	5.90	25.438	2957.9	7.192	Superheated	818.32	2910.4
D	250	5.90	3.649	2957.9	7.1915	Superheated	818.32	-
E	250	5.90	21.789	2957.9	7.1915	Superheated	818.32	-
F	154	1.20	0.875	2783.1	7.5467	Superheated	537.64	2642.9
G	34.91	0.056	20.914	2375.8	7.7412	0.922***	72.28	2315.8

* According to Fig. 1 and Fig. 2

** At the base ambient state (ambient pressure = 1 bar, ambient temperature = 25 °C)

*** Quality of 0.922 denotes 92.2% of steam and 7.8% of water droplets

Table A3 Steam operating parameters at LOAD 3

Operating Point*	Temperature (°C)	Pressure (bar)	Mass flow rate (kg/s)	Specific enthalpy (kJ/kg)	Specific entropy (kJ/kg·K)	Quality	Specific exergy (kJ/kg)**	Isentropic specific enthalpy (kJ/kg)
A	500.0	58.99	26.718	3424.3	6.8916	Superheated	1374.1	-
B	350.0	15.65	0.908	3146.7	7.0824	Superheated	1039.7	3032.8
C	256.4	5.93	25.810	2971.2	7.2145	Superheated	824.78	2903.4
D	256.4	5.93	3.658	2971.2	7.2145	Superheated	824.78	-
E	256.4	5.93	22.152	2971.2	7.2145	Superheated	824.78	-
F	153.0	1.21	0.904	2781.1	7.5381	Superheated	538.14	2653.0
G	34.91	0.056	21.248	2373.3	7.7334	0.921***	72.20	2313.2

* According to Fig. 1 and Fig. 2

** At the base ambient state (ambient pressure = 1 bar, ambient temperature = 25 °C)

*** Quality of 0.921 denotes 92.1% of steam and 7.9% of water droplets

Appendix B – measurement equipment

Table B1 List of used measurement equipment

Operating Point*	**Steam mass flow rate** [78]	**Steam pressure** [79]	**Steam temperature** [80]
A	Yamatake JTD960A	Yamatake JTG960A	Greisinger GTF 601-Pt100
B	Yamatake JTD960A	Yamatake JTG940A	Greisinger GTF 601-Pt100
C	Yamatake JTD930A	Yamatake JTG940A	Greisinger GTF 401-Pt100
D	Yamatake JTD930A	Yamatake JTG940A	Greisinger GTF 401-Pt100
E	Yamatake JTD930A	Yamatake JTG940A	Greisinger GTF 401-Pt100
F	Yamatake JTD920A	Yamatake JTG940A	Greisinger GTF 401-Pt100
G	Yamatake JTD910A	Yamatake JTG940A	Greisinger GTF 401-Pt100

* According to Fig. 1 and Fig. 2

Funding: The research presented in the manuscript did not receive any external funding.

Acknowledgments: The research has been supported by the Croatian Science Foundation under the project IP-2022-10-2821.

Author Contributions: Conceptualization: I.P., V.M. and T.S.; Methodology: I.P. and D.P.; Data collection: I.P.; Data curation: I.P., T.S. and D.P.; Formal analyzes: I.P. and V.M.; Research: I.P., V.M., T.S. and D.P.; Writing; I.P., V.M., T.S. and D.P.; Review and editing: V.M. and T.S.; Supervision: I.P. and D.P.; Final approval: I.P., V.M., T.S. and D.P.

References

[1] Feng, Y., Wang, H., Gao, R., & Zhu, Y. (2019). A Zero-Dimensional Mixing Controlled Combustion Model for Real Time Performance Simulation of Marine Two-Stroke Diesel Engines. Energies, 12(10), 2000. (doi:10.3390/en12102000)

[2] Zhang, Y., Xia, C., Liu, D., Zhu, Y., & Feng, Y. (2023). Experimental investigation of the high-pressure SCR reactor impact on a marine two-stroke diesel engine. Fuel, 335, 127064. (doi:10.1016/j.fuel.2022.127064)

[3] Cao, J., Li, T., & Zhou, X. (2021). A study of smart thermal insulation coating on improving thermal efficiency in a marine two-stroke low-speed diesel engine. Fuel, 304, 120760. (doi:10.1016/j.fuel.2021.120760)

[4] Lu, D., Theotokatos, G., Zhang, J., Zeng, H., & Cui, K. (2022). Parametric investigation of a large marine two-stroke diesel engine equipped with exhaust gas recirculation and turbocharger cut out systems. Applied Thermal Engineering, 200, 117654. (doi:10.1016/j.applthermaleng.2021.117654)

[5] Muše, A., Jurić, Z., Račić, N., & Radica, G. (2020). Modelling, performance improvement and emission reduction of large two-stroke diesel engine using multi-zone combustion model. Journal of Thermal Analysis and Calorimetry, 1-14. (doi:10.1007/s10973-020-09321-7)

[6] Balz, R., von Rotz, B., & Sedarsky, D. (2020). In-nozzle flow and spray characteristics of large two-stroke marine diesel fuel injectors. Applied Thermal Engineering, 180, 115809. (doi:10.1016/j.applthermaleng.2020.115809)

[7] Park, S., Kim, Y., Woo, S., & Lee, K. (2017). Optimization and calibration strategy using design of experiment for a diesel engine. Applied Thermal Engineering, 123, 917-928. (doi:10.1016/j.applthermaleng.2017.05.171)

[8] Ramesh, N., & Mallikarjuna, J. M. (2017). Low temperature combustion strategy in an off-highway diesel engine–experimental and CFD study. Applied Thermal Engineering, 124, 844-854. (doi:10.1016/j.applthermaleng.2017.06.078)

[9] Mrzljak, V., Žarković, B., & Poljak, I. (2017). Fuel mass flow variation in direct injection diesel engine–influence on the change of the main engine operating parameters. Pomorstvo, 31(2), 119-127. (doi:10.31217/p.31.2.6)

[10] He, Y., & Rutland, C. J. (2002). Modeling of a turbocharged di diesel engine using artificial neural networks. SAE Transactions, 1532-1543.

[11] Wang, G., Yu, W., Li, X., Su, Y., Yang, R., & Wu, W. (2019). Experimental and numerical study on the influence of intake swirl on fuel spray and in-cylinder combustion characteristics on large bore diesel engine. Fuel, 237, 209-221. (doi:10.1016/j.fuel.2018.09.156)

[12] Taghavifar, H., & Mazari, F. (2022). 1D diesel engine cycle modeling integrated with MOPSO optimization for improved NOx control and pressure boost. Energy, 247, 123517. (doi:10.1016/j.energy.2022.123517)

[13] Huang, M., Gowdagiri, S., Cesari, X. M., & Oehlschlaeger, M. A. (2016). Diesel engine CFD simulations: Influence of fuel variability on ignition delay. Fuel, 181, 170-177. (doi:10.1016/j.fuel.2016.04.137)

[14] Asadi, A., Kadijani, O. N., Doranehgard, M. H., Bozorg, M. V., Xiong, Q., Shadloo, M. S., & Li, L. K. (2020). Numerical study on the application of biodiesel and bioethanol in a multiple injection diesel engine. Renewable Energy, 150, 1019-1029. (doi:10.1016/j.renene.2019.11.088)

[15] Rajak, U., Nashine, P., Singh, T. S., & Verma, T. N. (2018). Numerical investigation of performance, combustion and emission characteristics of various biofuels. Energy Conversion and Management, 156, 235-252. (doi:10.1016/j.enconman.2017.11.017)

[16] Channapattana, S. V., Pawar, A. A., & Kamble, P. G. (2017). Optimisation of operating parameters of DI-CI engine fueled with second generation Bio-fuel and development of ANN based prediction model. Applied energy, 187, 84-95. (doi:10.1016/j.apenergy.2016.11.030)

[17] Sartomo, A., Santoso, B., & Muraza, O. (2020). Recent progress on mixing technology for water-emulsion fuel: A review. Energy Conversion and Management, 213, 112817. (doi:10.1016/j.enconman.2020.112817)

[18] Lamas Galdo, M. I., Castro-Santos, L., & Rodriguez Vidal, C. G. (2020). Numerical analysis of NOx reduction using ammonia injection and comparison with water injection. Journal of Marine Science and Engineering, 8(2), 109. (doi:10.3390/jmse8020109)

[19] Senčić, T., Mrzljak, V., Blecich, P., & Bonefačić, I. (2019). 2D CFD simulation of water injection strategies in a large marine engine. Journal of Marine Science and Engineering, 7(9), 296. (doi:10.3390/jmse7090296)

[20] Marques, C. H., Caprace, J. D., Belchior, C. R., & Martini, A. (2019). An Approach for Predicting the Specific Fuel Consumption of Dual-Fuel Two-Stroke Marine Engines. Journal of Marine Science and Engineering, 7(2), 20. (doi:10.3390/jmse7020020)

[21] Gospić, I., Glavan, I., Poljak, I., & Mrzljak, V. (2021). Energy, economic and environmental effects of the marine diesel engine trigeneration energy systems. Journal of marine science and engineering, 9(7), 773. (doi:10.3390/jmse9070773)

[22] Ammar, N. R. (2019). Environmental and cost-effectiveness comparison of dual fuel propulsion options for emissions reduction onboard LNG carriers. Brodogradnja: Teorija i praksa brodogradnje i pomorske tehnike, 70(3), 61-77. (doi:10.21278/brod70304)

[23] Fernández, I. A., Gómez, M. R., Gómez, J. R., & Insua, Á. B. (2017). Review of propulsion systems on LNG carriers. Renewable and Sustainable Energy Reviews, 67, 1395-1411. (doi:10.1016/j.rser.2016.09.095)

[24] Jelić, M., Mrzljak, V., Radica, G., & Račić, N. (2021). An alternative and hybrid propulsion for merchant ships: Current state and perspective. Energy Sources, Part A: Recovery, Utilization, and Environmental Effects, 1-33. (doi:10.1080/15567036.2021.1963354)

[25] Raj, R., Ghandehariun, S., Kumar, A., Geng, J., & Linwei, M. (2016). A techno-economic study of shipping LNG to the Asia-Pacific from Western Canada by LNG carrier. Journal of Natural Gas Science and Engineering, 34, 979-992. (doi:10.1016/j.jngse.2016.07.024)

[26] Ahn, J., Noh, Y., Park, S. H., Choi, B. I., & Chang, D. (2017). Fuzzy-based failure mode and effect analysis (FMEA) of a hybrid molten carbonate fuel cell (MCFC) and gas turbine system for marine propulsion. Journal of Power Sources, 364, 226-233. (doi:10.1016/j.jpowsour.2017.08.028)

[27] Budiyanto, M. A., & Nawara, R. (2020). The optimization of exergoenvironmental factors in the combined gas turbine cycle and carbon dioxide cascade to generate power in LNG tanker ship. Energy Conversion and Management, 205, 112468. (doi:10.1016/j.enconman.2020.112468)

[28] Jeong, B., Oguz, E., Wang, H., & Zhou, P. (2018). Multi-criteria decision-making for marine propulsion: Hybrid, diesel electric and diesel mechanical systems from cost-environment-risk perspectives. Applied Energy, 230, 1065-1081. (doi:10.1016/j.apenergy.2018.09.074)

[29] Jeong, B., Wang, H., Oguz, E., & Zhou, P. (2018). An effective framework for life cycle and cost assessment for marine vessels aiming to select optimal propulsion systems. Journal of Cleaner Production, 187, 111-130. (doi:10.1016/j.jclepro.2018.03.184)

[30] Koroglu, T., & Sogut, O. S. (2018). Conventional and advanced exergy analyses of a marine steam power plant. Energy, 163, 392-403. (doi:10.1016/j.energy.2018.08.119)

[31] Mrzljak, V., Poljak, I., & Medica-Viola, V. (2017). Dual fuel consumption and efficiency of marine steam generators for the propulsion of LNG carrier. Applied Thermal Engineering, 119, 331-346. (doi:10.1016/j.applthermaleng.2017.03.078)

[32] Chang, D., Rhee, T., Nam, K., Chang, K., Lee, D., & Jeong, S. (2008). A study on availability and safety of new propulsion systems for LNG carriers. Reliability Engineering & System Safety, 93(12), 1877-1885. (doi:10.1016/j.ress.2008.03.013)

[33] Figari, M., Theotokatos, G., Coraddu, A., Stoumpos, S., & Mondella, T. (2022). Parametric investigation and optimal selection of the hybrid turbocharger system for a large marine four-stroke dual-fuel engine. Applied Thermal Engineering, 208, 117991. (doi:10.1016/j.applthermaleng.2021.117991)

[34] Ma, C., Yao, C., Song, E. Z., & Ding, S. L. (2022). Prediction and optimization of dual-fuel marine engine emissions and performance using combined ANN with PSO algorithms. International Journal of Engine Research, 23(4), 560-576. (doi:10.1177/1468087421990476)

[35] Theotokatos, G., Stoumpos, S., Bolbot, V., & Boulougouris, E. (2020). Simulation-based investigation of a marine dual-fuel engine. Journal of Marine Engineering & Technology, 19(sup1), 5-16. (doi:10.1080/20464177.2020.1717266)

[36] Kaushik, S. C., Reddy, V. S., & Tyagi, S. K. (2011). Energy and exergy analyses of thermal power plants: A review. Renewable and Sustainable energy reviews, 15(4), 1857-1872. (doi:10.1016/j.rser.2010.12.007)

[37] Khaleel, O. J., Ismail, F. B., Ibrahim, T. K., & bin Abu Hassan, S. H. (2022). Energy and exergy analysis of the steam power plants: A comprehensive review on the Classification, Development, Improvements, and configurations. Ain Shams Engineering Journal, 13(3), 101640. (doi:10.1016/j.asej.2021.11.009)

[38] Fadhil, A. N., Shihab, A. P. A. S., & Faisal, S. H. (2017). Assessment of AL-Hartha Steam Power Station Using Energy and Exergy Analysis. International Journal of Modern Studies in Mechanical Engineering, 3(2), 17-30. (doi:10.20431/2454-9711.0302003)

[39] Hoseinzadeh, S., & Stephan Heyns, P. (2021). Advanced energy, exergy, and environmental (3E) analyses and optimization of a coal-fired 400 MW thermal power plant. Journal of Energy Resources Technology, 143(8), 082106. (doi:10.1115/1.4048982)

[40] Hafdhi, F., Khir, T., Yahyia, A. B., & Brahim, A. B. (2015). Energetic and exergetic analysis of a steam turbine power plant in an existing phosphoric acid factory. Energy Conversion and Management, 106, 1230-1241. (doi:10.1016/j.enconman.2015.10.044)

[41] Agrež, M., Avsec, J., & Strušnik, D. (2020). Entropy and exergy analysis of steam passing through an inlet steam turbine control valve assembly using artificial neural net-

works. International Journal of Heat and Mass Transfer, 156, 119897. (doi:10.1016/j.ijheatmasstransfer.2020.119897)

[42] Mrzljak, V., Jelić, M., Poljak, I., & Prpić-Oršić, J. (2023). Analysis and comparison of main steam turbines from four different thermal power plants. Pomorstvo, 37(1), 58-74. (doi:10.31217/p.37.1.6)

[43] Mrzljak, V., Poljak, I., & Mrakovčić, T. (2017). Energy and exergy analysis of the turbo-generators and steam turbine for the main feed water pump drive on LNG carrier. Energy conversion and management, 140, 307-323. (doi:10.1016/j.enconman.2017.03.007)

[44] Çiçek, A. N. (2009). Exergy analysis of a crude oil carrier steam plant. MSc. Thesis (in Turkish), Istanbul, Istanbul Technical University.

[45] Anđelić, N., Mrzljak, V., Lorencin, I., & Baressi Šegota, S. (2020). Comparison of exergy and various energy analysis methods for a main marine steam turbine at different loads. Pomorski zbornik, 59(1), 9-34. (doi:10.18048/2020.59.01)

[46] Malin, M. R. (1997). Modelling flow in an experimental marine condenser. International communications in heat and mass transfer, 24(5), 597-608. (doi:10.1016/S0735-1933(97)00046-8)

[47] Laskowski, R. (2016). Relations for steam power plant condenser performance in off-design conditions in the function of inlet parameters and those relevant in reference conditions. Applied Thermal Engineering, 103, 528-536. (doi:10.1016/j.applthermaleng.2016.04.127)

[48] Park, Y. G., Yoon, S. Y., Seo, Y. M., Ha, M. Y., Park, Y. M., & Koo, B. S. (2020). A study on the optimal arrangement of tube bundle for the performance enhancement of a steam turbine surface condenser. Applied Thermal Engineering, 166, 114681. (doi:10.1016/j.applthermaleng.2019.114681)

[49] Lisowski, E., & Rajda, J. (2013). CFD analysis of pressure loss during flow by hydraulic directional control valve constructed from logic valves. Energy Conversion and Management, 65, 285-291. (doi:10.1016/j.enconman.2012.08.015)

[50] Liu, X., Wu, Z., Li, B., Zhao, J., He, J., Li, W., ... & Xie, F. (2020). Influence of inlet pressure on cavitation characteristics in regulating valve. Engineering Applications of Computational Fluid Mechanics, 14(1), 299-310. (doi:10.1080/19942060.2020.1711811)

[51] McBirnie, S. C. (2013). Marine, Steam Engines, and Turbines. Elsevier.

[52] Carlton, J. (2018). Marine propellers and propulsion. Butterworth-Heinemann.

[53] Kostyuk, A., & Frolov, V. (Eds.). (1988). Steam and gas turbines. Mir Pub.

[54] Adibhatla, S., & Kaushik, S. C. (2017). Exergy and thermoeconomic analyses of 500 MWe sub critical thermal power plant with solar aided feed water heating. Applied Thermal Engineering, 123, 340-352. (doi:10.1016/j.applthermaleng.2017.05.099)

[55] Kanoğlu, M., Çengel, Y. A., & Dinçer, İ. (2012). Efficiency evaluation of energy systems. Springer Science & Business Media.

[56] Poljak, I., & Mrzljak, V. (2023). Thermodynamic Analysis and Comparison of Two Marine Steam Propulsion Turbines. NAŠE MORE: znanstveni časopis za more i pomorstvo, 70(2), 0-0. (doi:10.17818/NM/2023/2.2)

[57] Elčić, Z. (1995). Steam turbines. ABB, Karlovac, National and University Library Zagreb.

[58] Noroozian, A., Mohammadi, A., Bidi, M., & Ahmadi, M. H. (2017). Energy, exergy and economic analyses of a novel system to recover waste heat and water in steam power plants. Energy conversion and management, 144, 351-360. (doi:10.1016/j.enconman.2017.04.067)

[59] Dincer, I., & Rosen, M. A. (2012). Exergy: energy, environment and sustainable development. Newnes.

[60] Taheri, M. H., Mosaffa, A. H., & Farshi, L. G. (2017). Energy, exergy and economic assessments of a novel integrated biomass based multigeneration energy system with hydrogen production and LNG regasification cycle. Energy, 125, 162-177. (doi:10.1016/j.energy.2017.02.124)

[61] Abou Houran, M., Nutakki, T. U. K., Albani, A., Ifseisi, A. A., Riaz, F., & Peng, F. (2024). Energy and exergy analysis of a novel solar-based system merged with power cycle. Applied Thermal Engineering, 240, 122080. (doi:10.1016/j.applthermaleng.2023.122080)

[62] Eboh, F. C., Ahlström, P., & Richards, T. (2017). Exergy analysis of solid fuel-fired heat and power plants: a review. Energies, 10(2), 165. (doi:10.3390/en10020165)

[63] Mrzljak, V., Poljak, I., Jelić, M., & Prpić-Oršić, J. (2023). Thermodynamic Analysis and Improvement Potential of Helium Closed Cycle Gas Turbine Power Plant at Four Loads. Energies, 16(15), 5589. (doi:10.3390/en16155589)

[64] Aljundi, I. H. (2009). Energy and exergy analysis of a steam power plant in Jordan. Applied thermal engineering, 29(2-3), 324-328. (doi:10.1016/j.applthermaleng.2008.02.029)

[65] Mahian, O., Mirzaie, M. R., Kasaeian, A., & Mousavi, S. H. (2020). Exergy analysis in combined heat and power systems: A review. Energy conversion and management, 226, 113467. (doi:10.1016/j.enconman.2020.113467)

[66] Tan, H., Shan, S., Nie, Y., & Zhao, Q. (2018). A new boil-off gas re-liquefaction system for LNG carriers based on dual mixed refrigerant cycle. Cryogenics, 92, 84-92. (doi:10.1016/j.cryogenics.2018.04.009)

[67] Szargut, J. (2005). Exergy method: technical and ecological applications (Vol. 18). WIT press.

[68] Ahmadi, G. R., & Toghraie, D. (2016). Energy and exergy analysis of Montazeri steam power plant in Iran. Renewable and Sustainable Energy Reviews, 56, 454-463. (doi:10.1016/j.rser.2015.11.074)

[69] Maruf, M. H., Rabbani, M., Ashique, R. H., Islam, M. T., Nipun, M. K., Haq, M. A. U., ... & Shihavuddin, A. S. M. (2021). Exergy based evaluation of power plants for sustainability and economic performance identification. Case Studies in Thermal Engineering, 28, 101393. (doi:10.1016/j.csite.2021.101393)

[70] Adibhatla, S., & Kaushik, S. C. (2014). Energy and exergy analysis of a super critical thermal power plant at various load conditions under constant and pure sliding pressure operation. Applied thermal engineering, 73(1), 51-65. (doi:10.1016/j.applthermaleng.2014.07.030)

[71] Ameri, M., Mokhtari, H., & Sani, M. M. (2018). 4E analyses and multi-objective optimization of different fuels application for a large combined cycle power plant. Energy, 156, 371-386. (doi:10.1016/j.energy.2018.05.039)

[72] Erdem, H. H., Akkaya, A. V., Cetin, B., Dagdas, A., Sevilgen, S. H., Sahin, B., ... & Atas, S. (2009). Comparative energetic and exergetic performance analyses for coal-fired thermal power plants in Turkey. International Journal of Thermal Sciences, 48(11), 2179-2186. (doi:10.1016/j.ijthermalsci.2009.03.007)

[73] Lemmon, E. W., Huber, M. L., & McLinden, M. O. (2010). NIST Standard Reference Database 23, Reference Fluid Thermodynamic and Transport Properties (REFPROP), version 9.0, National Institute of Standards and Technology. R1234yf. fld file dated December, 22, 2010.

[74] Mrzljak, V., Poljak, I., Prpić-Oršić, J., & Jelić, M. (2020). Exergy analysis of marine waste heat recovery CO2 closed-cycle gas turbine system. Pomorstvo, 34(2), 309-322. (doi:10.31217/p.34.2.12)

[75] Mrzljak, V., Poljak, I., & Prpić-Oršić, J. (2019). Exergy analysis of the main propulsion steam turbine from marine propulsion plant. Brodogradnja: Teorija i praksa brodogradnje i pomorske tehnike, 70(1), 59-77. (doi:10.21278/brod70105)

[76] Kopac, M., & Hilalci, A. (2007). Effect of ambient temperature on the efficiency of the regenerative and reheat Çatalağzı power plant in Turkey. Applied Thermal Engineering, 27(8-9), 1377-1385. (doi:10.1016/j.applthermaleng.2006.10.029)

[77] Khajehpour, H., Norouzi, N., & Fani, M. (2021). An exergetic model for the ambient air temperature impacts on the combined power plants and its management using the genetic algorithm. International Journal of Air-Conditioning and Refrigeration, 29(01), 2150008. (doi:10.1142/S2010132521500085)

[78] http://www.krtproduct.com (accessed: 11.03.2024)

[79] http://www.industriascontrolpro.com (accessed: 11.03.2024)

[80] https://www.greisinger.de (accessed: 12.03.2024)